Supporting Information

Supporting Information Corrected November 20, 2012

Lu et al. 10.1073/pnas.1208642109

SI Materials and Methods

Constructs and Protein Expression. The coding sequence of myosin X (Myo10) (NP_036466.2, residues 813–962) was PCR-amplified from human Myo10 and cloned into a pET32a vector. Protein was expressed in BL21(DE3) *Escherichia coli* cells. The His_6-tagged proteins were purified using a Ni^{2+}-nitrilotriacetic acid agarose column followed by size-exclusion chromatography.

The GFP-tagged full-length Myo10 expression plasmid (NP_036466.2, 1–2058, provided by Wencheng Xiong, Georgia Health Sciences University, Augusta, GA) is referred to as Motor-CC(WT)-Tail. The truncation constructs labeled as Motor-single α-helix (SAH) refers to coding sequence from 1 to 855 containing motor, IQ, and SAH. Motor-CC(1-934)(WT) refers to residue 1–934. GCN4 sequence QLEDKVEELLSKNYHLENEVARLKKLVGE was used to substitute coiled coil at residue 849–934 and labeled as Motor-SAH-GCN4 and Motor-SAH-GCN4-Tail, respectively. Point mutations of Myo10 constructs were created by PCR-based mutagenesis.

NMR Spectroscopy. NMR samples contained 0.8 mM of the Myo10 in 100 mM potassium phosphate (pH 6.5, with 1 mM DTT, 1 mM EDTA) in 90% H_2O/10% D_2O or 99.9% (vol/vol) D_2O. NMR spectra were acquired at 30 °C on Varian Inova 750- and 800-MHz spectrometers, each equipped with an actively *z*-gradient shielded triple resonance probe. Backbone and side-chain resonance assignments of Myo10 were achieved by the standard heteronuclear correlation experiments (1). Spectra were processed using the NMRPipe software (2) and analyzed with PIPP (3).

NMR Structural Calculation. The present structure is based on the experimental distance and torsional angle restraints determined from a suite of 3D ^{13}C- and ^{15}N-separated NOESY experiments using a mixing time of 100 ms. Hydrogen bonding restraints were generated from the standard secondary structure of the protein based on the NOE patterns and backbone secondary chemical shifts. The backbone dihedral angle restraints (φ and ψ angles) were derived from the chemical shift analysis program TALOS (4).

The structural determination of Myo10 antiparallel coiled coil (anti-CC) was completed in a stepwise manner. At the initial steps, we used only 309 definitive intramolecular NOEs (e.g., those described in Fig. 2*C* and Fig. S4), and the rest of the NOEs were all treated as ambiguous NOEs for the structural calculation. We were able to obtain a highly converged, antiparallel-oriented Myo10 coiled-coil structure with these 309 intramolecular NOEs. After this step, numerous NOEs can be safely assigned as intermolecular NOEs on the basis of their distances indicated by these initial antiparallel dimer structure models. Such exercises were iterated for multiple cycles until the structure was highly converged with good stereo-chemical criteria.

For the residues in the center region, it is impossible to determine whether their NOEs are intra- and intermolecular in nature. These NOEs were treated as ambiguous NOE restraints (i.e., either intra- or intermolecular couplings). At the final step of the structural calculation, a total of 659 intermolecular NOEs were assigned, and 382 NOEs were included as ambiguous NOEs (Table 1).

Structures were calculated using the program CNS (2). Figures were generated using PYMOL (http://pymol.sourceforge.net/) and MOLMOL (3). The program Procheck (5) was used to assess the overall quality of the structures. Ramachandran statistics for the final ensemble of structures for residues 883–925 of the Myo10 antiparallel coiled coil show that 95.4% of residues are in the most favored region, 4.0% of the residues are in the additionally allowed region, and 0.6% of the residues are in the generally allowed region. None of the structures exhibits distance violations greater than 0.3 Å or dihedral angle violations greater than 4°.

Analytical Ultracentrifugation. Sedimentation velocity experiments were performed on a Beckman XL-I analytical ultracentrifuge equipped with an eight-cell rotor at 25 °C. The partial specific volume of protein samples and the buffer density were calculated using the program SEDNTERP (www.rasmb.bbri.org). The final sedimentation velocity data were analyzed using the program SEDFIT (www.analyticalultracentrifugation.com) and fitted to a continuous sedimentation coefficient distribution model.

Sedimentation equilibrium experiments were performed using a Beckman proteomelab XL-I ultracentrifuge equipped with Beckman 50Ti rotor and six sector cells at three different concentrations: 20, 40, and 60 μM. Different boundaries of the thioredoxin (trx)-tagged Myo10 were centrifuged at 13,000 rpm on an An-50 Ti rotor. Samples were equilibrated for 72 h in the 13,000-rpm rotor speed setting, scans were taken every 12 h, and data were buffer-corrected. Data were analyzed by Sedfit and Sedphat programs (www.analyticalultracentrifugation.com/default.htm). Data fitting was performed using a monomer–dimer association model and with simulated annealing algorithms (6).

Cellular Localization and Filopodia Quantification. HeLa and COS7 cells were transiently transfected with 0.5 μg of each plasmid (12-well plate) per well using a lipofectamine PLUS kit (Invitrogen), and cells were cultured 16 h in DMEM containing 10% FBS in 10% CO_2 before fixation. Cells were imaged with a Nikon TE2000E inverted fluorescent microscope. Actin was stained by rhodamine-conjugated phalloidin (Invitrogen) to visualize filopodia. The number of filopodia (crossing the cell edge, phalloidin-positive with length >0.5 μm) and GFP puncta at the tip of filopodia were tracked and quantified by Metamorph software. Data were analyzed using a Student's *t* test. Typically, 10 cells were quantified for each construct, and values (means ± SD) were calculated from three independent experiments.

1. Bax A, Grzesiek S (1993) Methodological advances in protein NMR. *Acc Chem Res* 26: 131–138.
2. Delaglio F, et al. (1995) NMRPipe: A multidimensional spectral processing system based on UNIX pipes. *J Biomol NMR* 6:277–293.
3. Garrett DS, Powers R, Gronenborn AM, Clore GM (2011) A common sense approach to peak picking in two-, three-, and four-dimensional spectra using automatic computer analysis of contour diagrams. 1991. *J Magn Reson* 213:357–363.
4. Cornilescu G, Delaglio F, Bax A (1999) Protein backbone angle restraints from searching a database for chemical shift and sequence homology. *J Biomol NMR* 13: 289–302.
5. Laskowski RA, Macarthur MW, Moss DS, Thornton JM (1993) Procheck: A program to check the stereochemical quality of protein structures. *J Appl Cryst* 26:283–291.
6. Lebowitz J, Lewis MS, Schuck P (2002) Modern analytical ultracentrifugation in protein science: A tutorial review. *Protein Sci* 11:2067–2079.

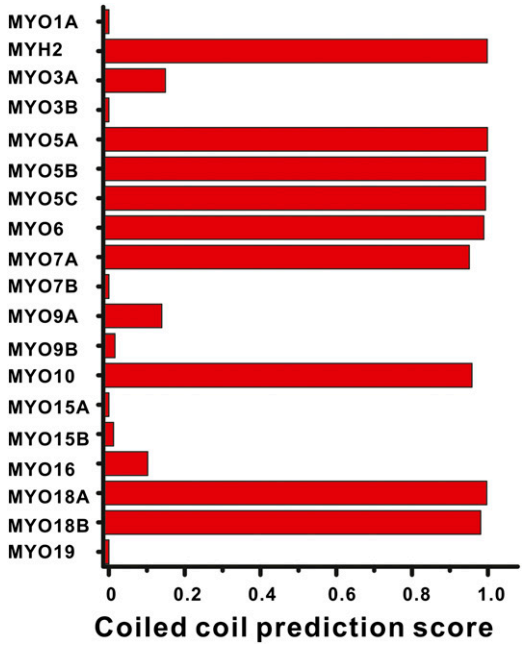

Fig. S1. Coiled-coil predictions of human myosins. The figure shows the highest coiled-coil formation score of a 200-residue fragment immediately after the C-terminal of the last IQ motif of each myosin. The prediction was performed by the Multicoil algorithm (http://groups.csail.mit.edu/cb/multicoil/). Only MYO1A and MYH2 for Myo1 and myosin II were selected to avoid excessive redundancy.

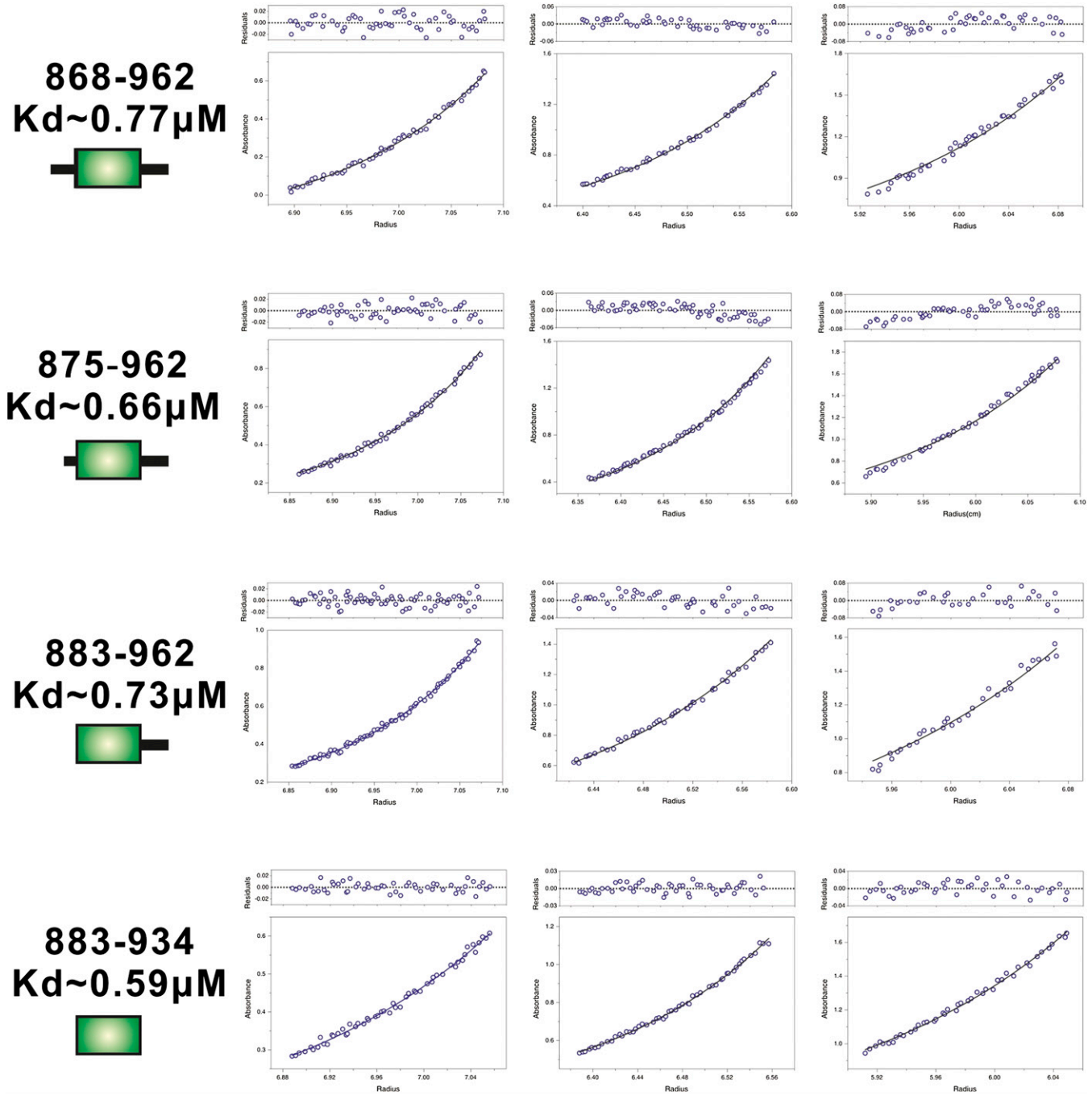

Fig. S2. Sedimentation equilibrium analysis of the dimerization strength of various Myo10 coiled-coil fragments. The figure shows the sedimentation profiles of four different fragments of Myo10 in 50 mM Tris buffer at pH 7.8 containing 100 mM NaCl and 1 mM DTT each at three different concentrations (absorption at 280 nm of 0.3, 0.6, and 1.2, respectively). The rotor speed for the sedimentation experiment was 13,000 rpm. The fitted dissociation constant (K_d) of the Myo10 coiled-coil dimer of four different fragments is comparable and around 0.6 μM. Sedimentation experiments were performed on a Beckman XL-I analytical ultracentrifuge equipped with an eight-cell rotor at 25 °C. Data were analyzed using Sedfit and Sedphat (www.analyticalultracentrifugation.com/default.htm). Global data fitting for three different concentrations were performed using a homodimer association model and simulated annealing algorithms.

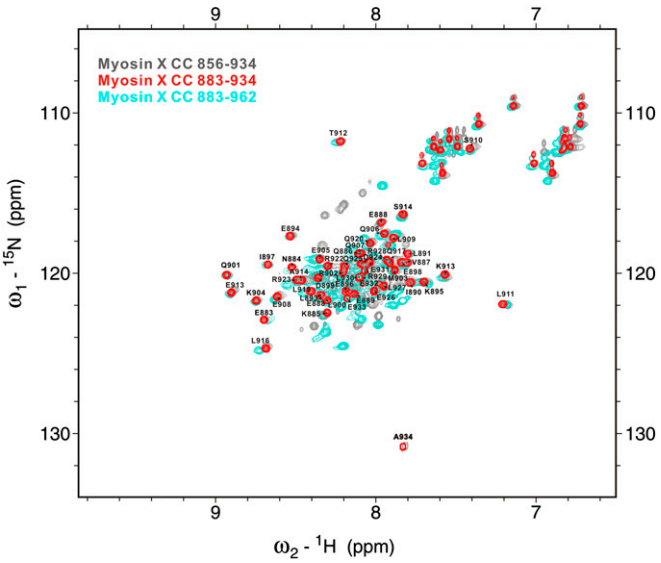

Fig. S3. The minimal dimer formation region of Myo10. Overlay plot of the ^{1}H-^{15}N hetero-nuclear single quantum coherence (HSQC) spectra of three different Myo10 coiled-coil fragments. The residues corresponding to residues 883–934 in the three samples can be nicely overlapped with each other, indicating that this fragment adopts the same conformation in these three constructs. Also, the ^{1}H-^{15}N HSQC spectrum of the minimal dimerization domain of Myo10 (aa 883–934) is well-dispersed and contains only one set of peaks, indicating that the domain forms a well-folded, symmetric dimer.

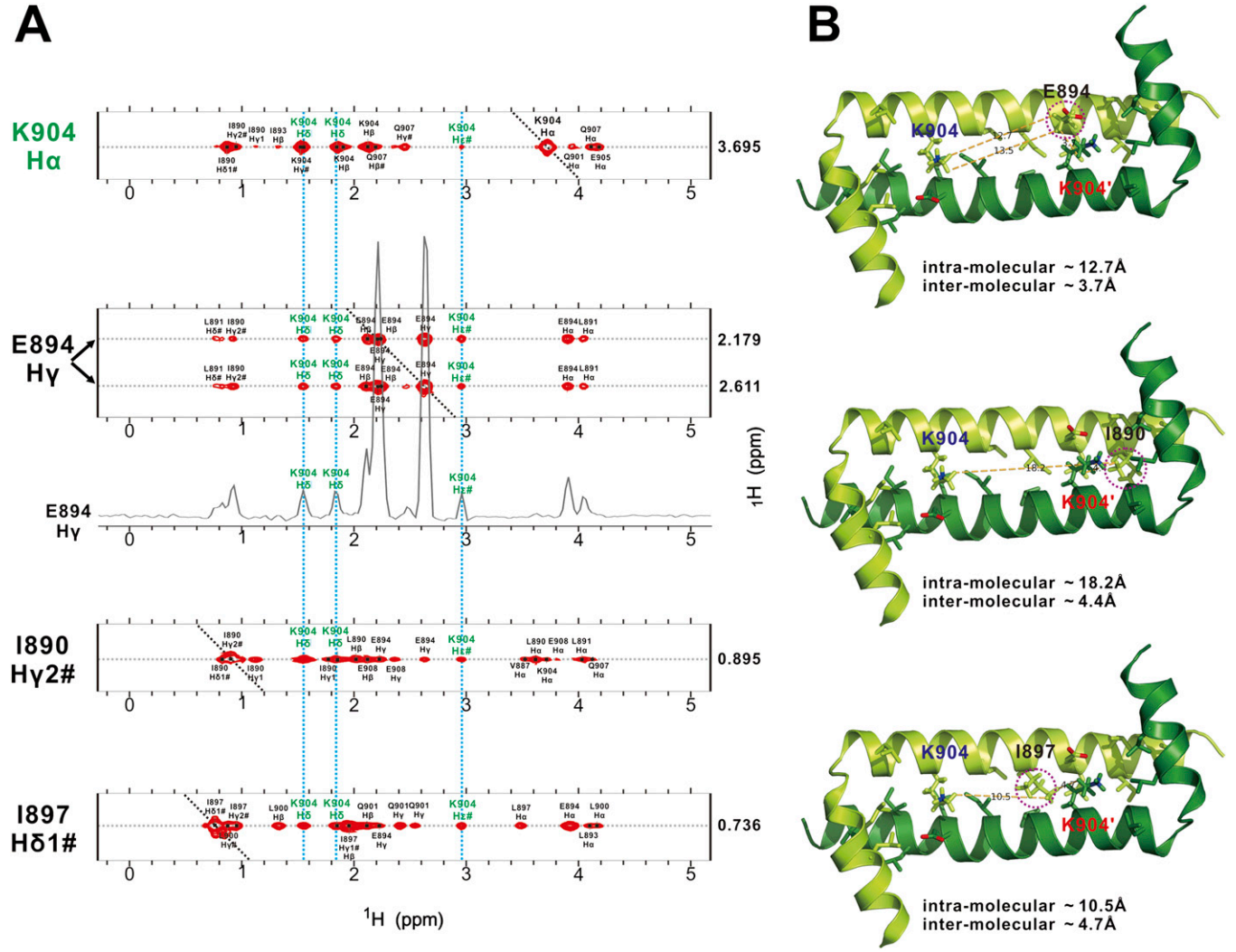

Fig. S4. Selected strips of 3D ^{13}C-NOESY spectrum showing definitive intermolecular NOEs of the anti-CC dimer. (*A*) Selected strips from the 3D ^{13}C-NOESY spectrum of Myo10 (aa 883–934) showing long-distance NOEs between the side chain of Lys904 with the side chains of Glu894, Ile890, and Ile897. To show data quality (both the signal-to-noise ratio, line shape of peaks, and baseline of the spectrum), a representative 1D slice (a γH of Glu894) is drawn. Diagonal peaks are indicated with dashed diagonal lines. (*B*) Ribbon diagram showing the positions of the corresponding amino acid residues shown in *A* in the Myo10 anti-CC dimer. The figure also shows the distances of the corresponding pair of protons if they are from the same molecule (i.e., intramolecular) or between two different molecules (i.e., intermolecular) of Myo10 (aa 883–934). This illustration shows that the long-range NOEs shown in *A* can only be intermolecular in nature, as the corresponding pairs of protons are much too far apart to have such NOEs.

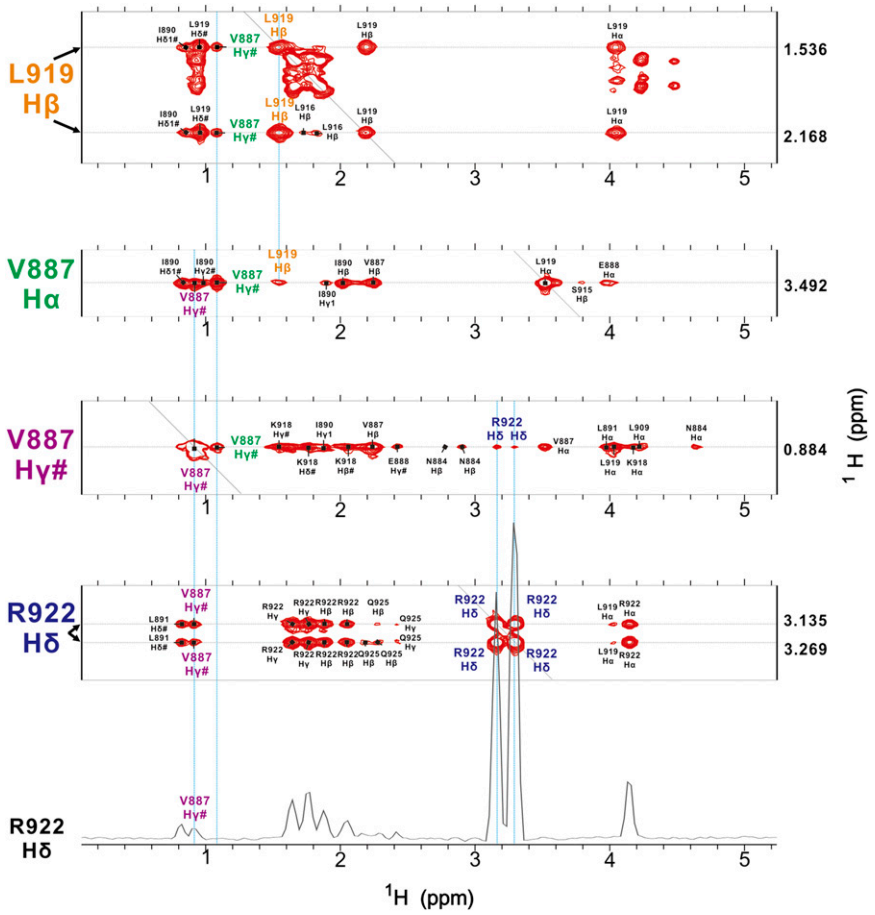

Fig. S5. Selected strips from the 3D ^{13}C-NOESY spectrum of Myo10 (aa 883–934) showing long-distance NOEs between side chain of Leu919 and Arg922 with the side chains of Val887.

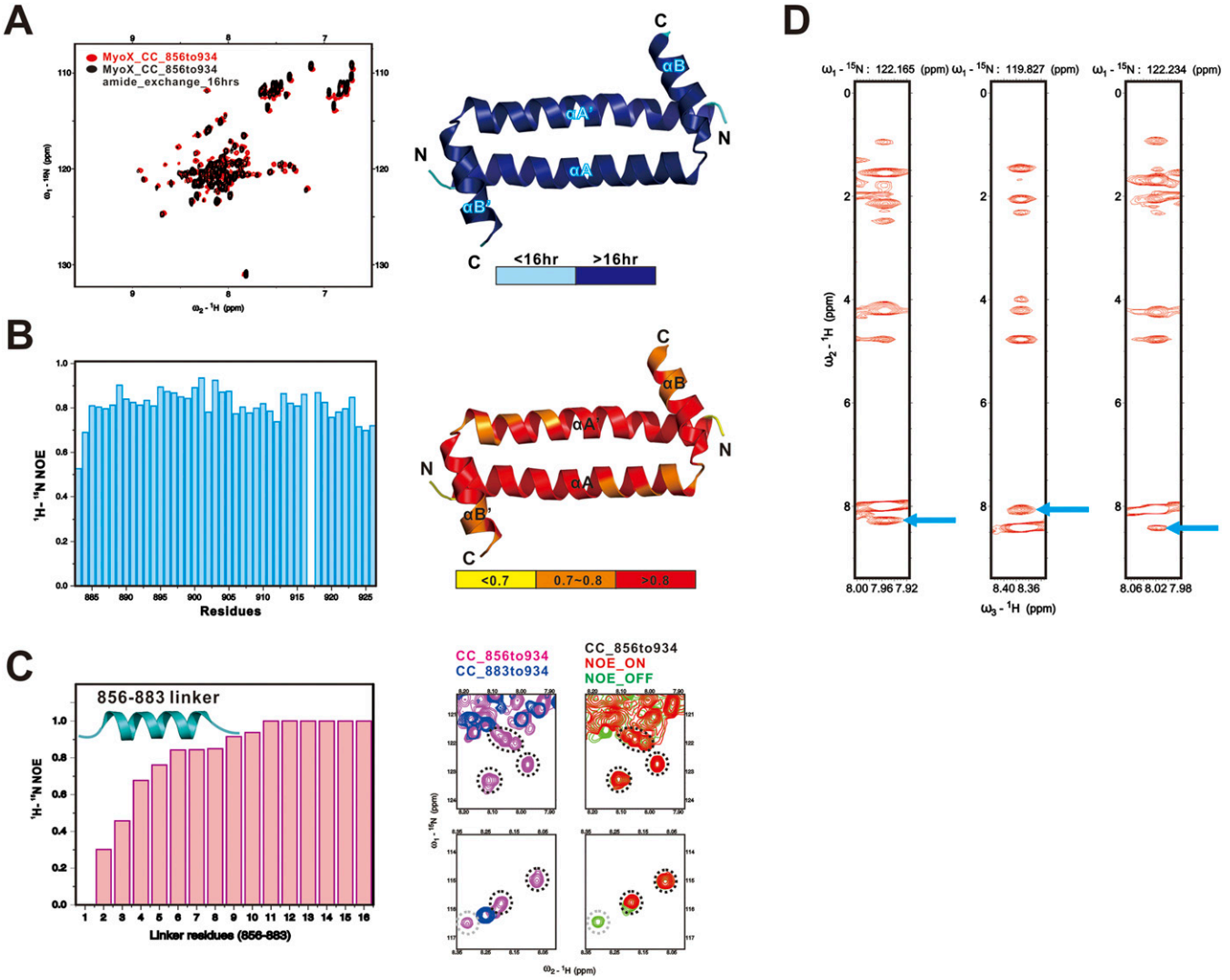

Fig. S6. Structural stability of the Myo10 anti-CC dimer. (*A*) NMR-based amide exchange experiment of Myo10 anti-CC (aa 856–934). The figure shows that the backbone amides corresponding to the anti-CC region are highly resistant to the H/D exchange. (*Right*) Essentially all of the amides from the residues in anti-CC of Myo10 are still protonated at 16 h after the initiation of the H/D exchange. (*B*) Plot of the steady-state ^{1}H-^{15}N NOE of the Myo10 anti-CC (aa 883–934) as the function of the residue number. The entire backbone of anti-CC is rigid as indicated by the large heteronuclear NOE values. (*Right*) The heteronuclear NOEs to the structure of the anti-CC dimer. (*C*) Heteronuclear steady-state ^{1}H-^{15}N NOE experiment of the linker connecting SAH and anti-CC (aa 856–882). More than 13 residues from this connection sequence (peaks highlighted with black dashed circles in the right panel) have large NOE values and adopt a semirigid, helix-like structure. There are also three residues from the connection sequence that have low NOE values (highlighted with gray dashed circles). Amide-exchange experiments were performed by dissolving a lyophilized, ^{15}*N*-labeled NMR sample in 99.9% D_2O and collecting series of ^{15}*N*-HSQC spectra at 10, 20, 60, 120, 240, 480, 720, and 960 min after the initiation of the exchange. Steady-state ^{1}H-^{15}N heteronuclear NOEs were measured on a 800-MHz spectrometer at 30 °C in triplicate by calculating the ratio of each amide peak volume with and without the presence of a 3-s proton presaturation pulse. (*D*) Selected strips from the 3D ^{15}*N*-NOESY spectrum of Myo10 (aa 846–934) showing dNN NOEs (indicated by arrowheads) of the NH group of the residues in the linker between SAH and anti-CC.

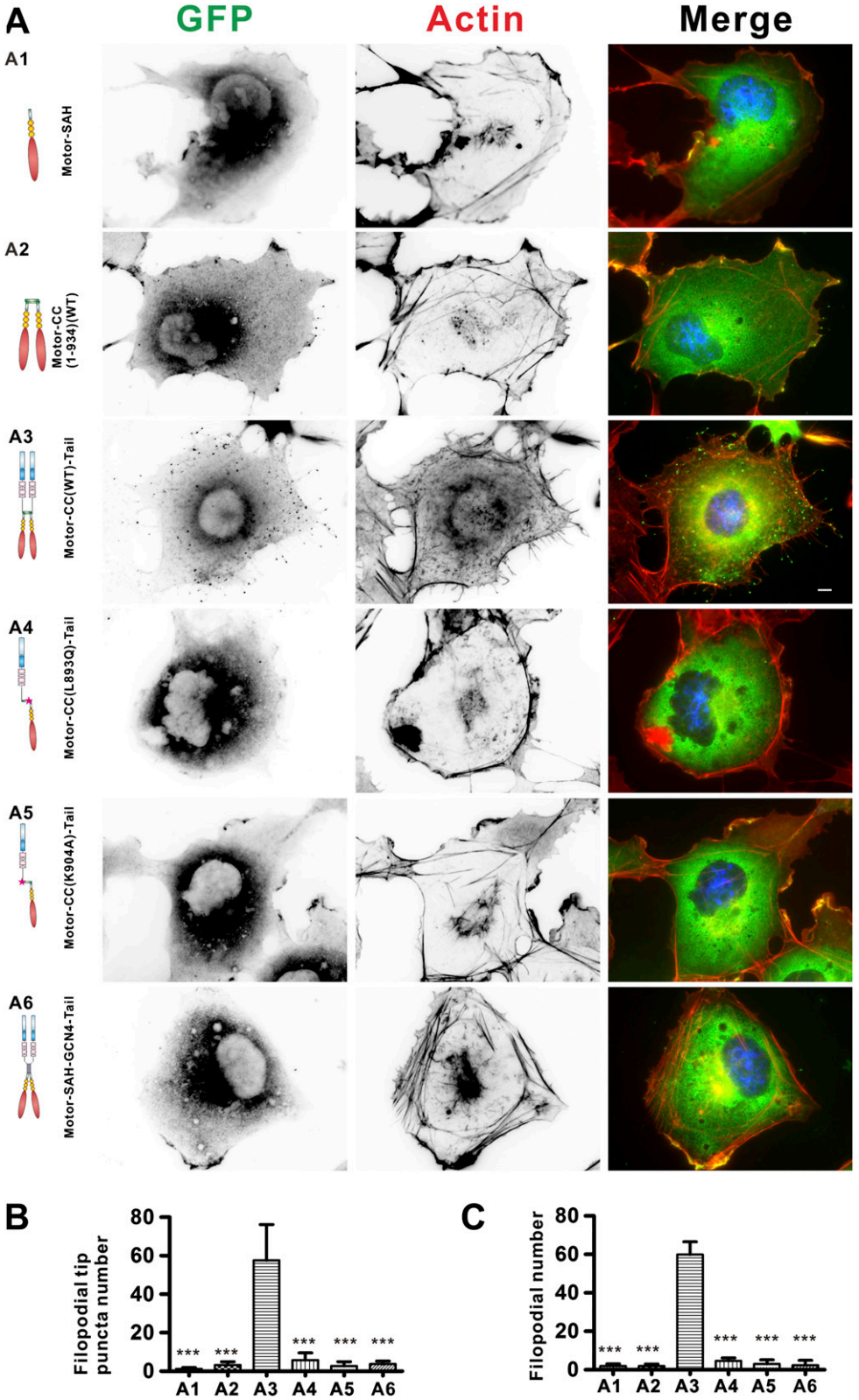

Fig. S7. The anti-CC of Myo10 is required for the motor's filopodial induction activity in COS7 cells. (*A*) Representative images of COS7 cells transfected with various GFP-tagged Myo10 constructs. In these images, actin filaments were stained with phalloidin (red), and nuclei were stained with DAPI (blue). (*A1*), Motor-SAH; (*A2*), Motor-CC(1-934)(WT); (*A3*), Motor-CC(WT)-Tail; (*A4*), Motor-CC(L893Q)-Tail; (*A5*), Motor-CC(K904A)-Tail; (*A6*), Motor-SAH-GCN4-Tail. (Scale bar, 5 μm.) (*B* and *C*) Quantitative analysis of GFP puncta number per cell at the tip of filopodia (*B*) and filopodial number (*C*) (with length >0.5 μm). Values are means ± SD from three independent experiments with 10 cells per experiment, using unpaired *t* test, $*P < 0.05$, $**P < 0.01$, $***P < 0.001$.

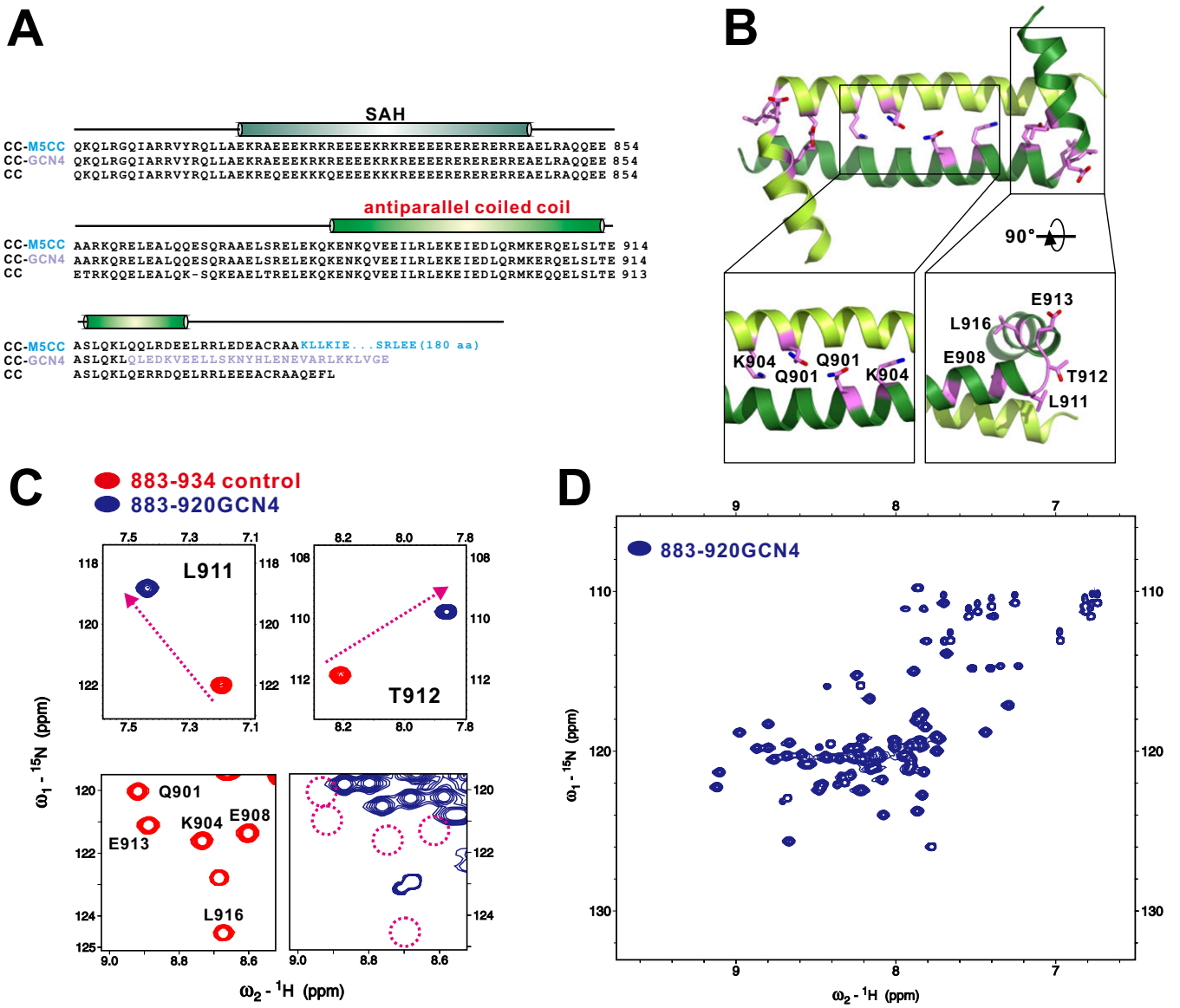

Fig. S8. (*A*) Details of the constructs of Myo10 used in this and previous studies. The sequence labeled with "CC-M5CC" was used in the study by Sun et al. with the coiled coil residues from Myo5 in purple (1), and the "CC-GCN4" was used by Nagy et al. with the GCN4 sequence in blue (2). The "CC" fragment in "CC-GCN4" used in this study is from bovine Myo10. (*B*) Mapping of the large chemical shift changes induced by fusing the GCN4 sequence at Leu920 of Myo10 αB on to the structure of Myo10 anti-CC. The residues experienced large backbone shift changes are drawn in the stick model. (*C*) Comparison of the HSQC spectrum of Myo10 anti-CC with that of anti–CC-GCN4 chimera. For clarity, only three selected regions of the spectra are shown. (*Upper*) The fusion of GCN4 led to very large chemical shift changes to the two residues in the αA/αB linker (Leu911 and Thr912), indicating a large interhelical angle change between αA and αB induced by the GCN4 fusion. (*Lower*) A number of well-resolved peaks from αA and αB (e.g., Gln901, Lys903, Glu913, and Leu916) underwent large shift changes (highlighted by the disappearances of these peaks in the *Right Lower* panel) induced by the GCN4 fusion. (*D*) The well-dispersed HSQC spectrum of CC-GCN4 indicates that CC-GCN4 still forms a dimer, albeit with obvious different conformation to that of the wild-type Myo10 anti-CC.

1. Sun Y, et al. (2010) Single-molecule stepping and structural dynamics of myosin X. *Nat Struct Mol Biol* 17:485–491.
2. Nagy S, et al. (2008) A myosin motor that selects bundled actin for motility. *Proc Natl Acad Sci USA* 105:9616–9620.